PRAMANA
— journal of
physics

© Printed in India

Vol. 42, No. 5,
May 1994
pp. 405–420

Electronic structure of non-magnetic impurities in dilute alloys of Al

P SINGH and S PRAKASH
Department of Physics, Panjab University, Chandigarh 160014, India

MS received 4 December 1993

Abstract. The electronic structure of substitutional non-magnetic impurities Cu, Ag, Cd, Mg, Zn, Ga, In, Ge, Si and Sn in Al is studied using density functional theory. A simple physical model is proposed to calculate the effective charges on impurities in trivalent metal Al. A linear relation is found between the effective charges on impurities and impurity vacancy capture radii. The spherical solid model (SSM) is used to account for discrete nature of the host. The impurity-induced change in charge density, scattering phase shifts, host-impurity potential, residual resistivity and impurity self-energy are calculated. Higher order scattering phase shifts are found significant and the host-impurity potential is found proportional to effective charge on impurity in its vicinity. The self-consistently calculated potential is used to calculate the electric field gradients (EFGs) at the first and second nearest neighbours (1NNs, 2NNs) of impurity. The calculated values are in agreement with the experimental results.

Keywords. EFG; defects; resistivity.

PACS Nos 71·50; 71·55

1. Introduction

The electronic structure of dilute alloys has been studied using jellium model of the metal and density functional theory [1, 2]. Manninen and Nieminen [3] replaced jellium model by SSM to include the discrete nature of lattice and investigated the magnetic structure of 3*d* impurities in Al [4]. Mahajan and Prakash [2] have included the size effect and Friedel criterion for bound states to determine the effective charges on impurities [2, 5] and the size effect was found significant in the calculation of impurity-induced charge density and host-impurity potential.

Prakash [6] used the model wavefunction transformation to study the impurity-induced charge density $\delta n_i(\mathbf{r})$ in a *d*-band metal. $\delta n_i(\mathbf{r})$ is separated into two parts: one due to non-nodal character of the wavefunction and other due to depletion hole around the host ions. Raj *et al* [7] used this $\delta n_i(\mathbf{r})$ to calculate the EFGs. Ponnambalam and Jena [8] used the asymptotic form of $\delta n_i(\mathbf{r})$ to calculate EFGs in Al alloys. However the size effect was ignored.

In all the above calculations either the SSM or the size effect was ignored. Recently we studied the electronic structure of non-magnetic impurities in dilute alloys of Cu [9] and hydrogen and muon in Al, Mg and Cu [10] including both the discrete nature of lattice and size effect. The host-impurity potentials are found proportional to the impurity charge in the vicinity of the impurity and Friedel oscillations are found at large distances. The virtual bound states of proton and muon are favoured in Al, Mg and Cu. The experimental results of residual resistivity and Knight shift

are explained. Therefore we found it interesting to extend the calculations for dilute alloys of Al for which lots of experimental data exist.

In the following we present the physical model for determining the impurity valencies, explanation of vacancy-impurity, capture radii of impurities, host-impurity potentials, induced charge densities, charge transfers, residual resistivities and EFGs in dilute alloys of Al.

2. Physical model

In a monovalent metal if the zero of the energy is taken as the energy of an electron at rest outside the metal, the bottom of the conduction band has the energy $-E_0$, which is given as

$$E_0 = E_s + E_1 + \tfrac{3}{5}E_F + E_{xc}. \tag{1}$$

Here sublimation energy E_s is the sum of molecular dissociation energy and work function, E_1 is the first ionization energy, $(3/5E_F)$ is the average kinetic energy and E_{xc} is the exchange-correlation energy of conduction electrons per electron. The energy required to dissociate the ith electron of the impurity atom in the lattice is

$$E_I \simeq E_i + E_{xc}, \tag{2}$$

where E_i is ith ionization potential of impurity atom and E_{xc} is the same as in (1). If $E_i \gg E(E = E_0 - E_{xc})$, the bound state will exist and the ith electron will not be dissociated in the lattice. If $E_i < E$, the ith electron of impurity atom will be added in the conduction band and the band structure of the host metal will be changed. This criterion has been found applicable to the monovalent metal Cu [9, 11].

In general it is assumed that Al is a trivalent metal. The E_0 given in (1) consists of only first ionization energy E_1, therefore E_0 does not represent the bottom of the conduction band in Al metal. Johnson and Martensson [12] calculated the core level binding energy shifts in the metal relative to the atom. The energy of different ionic configurations is about half of the corresponding ionization energy. Therefore replacement of E_1 by third ionization potential E_3 in (1) does not seem justified.

The detailed calculations of [12] suggest that the zero of energy should be renormalized to determine the realistic valencies of impurities in Al. This is essential as at least first ionization is needed to get the impurity dissolved. Therefore we choose E_0 as given in (1) as the reference energy. We further assume that ionization potentials, other than E_1, of the impurity atoms and Al atom are reduced in the same ratio in the solid solution. Thus we compare the ionization potentials E_2, E_3, E_4 of the impurity atoms with the corresponding potentials of Al atom [12]. If E_i of the impurity atom is less than E_i of Al atom, the ith electron of impurity atom is dissociated, otherwise the ith electron is the bound electron. According to this criterion Al atom in Al host is a trivalent interstitial which is required. These realistic valencies Z_I of impurities in Al host are given in table 1. The size effect is included in the same way as discussed earlier [9, 10]. The impurity valency Z_I is modified as

$$Z' = Z_I - \left(\frac{\Delta V}{V}\right) Z_H, \tag{3}$$

and the net charge on the impurity becomes

$$\Delta Z = Z' - Z_H. \tag{4}$$

Here $(\Delta V/V)$ is local dilation around impurity and Z_H is the host ionicity. The second term in (3) is due to lattice dilation. Equation (4) suggests that the net charge on self-interstitial atom is only due to lattice dilation.

We notice that Ag and Cu are monovalent and Mg and Zn are divalent impurities in Al. Since E_2 for Zn is just close to E_2 for Al, Zn may also be monovalent. However the polyvalent impurities In, Si, Ge, Sn and Cd are divalent except Ga which is monovalent. For the same reason as discussed for Zn, In and Si may also be monovalent. There are uncertainties about the ionization potentials of transition metal (TM) atoms. We have taken averaged values of ionization potentials [13]. Ti is trivalent while V and Cr are divalent. These impurities also consist of partially localized *d*-electrons. This effect is included implicitly in the determination of the bound state. We have taken the averaged value of available data for dilation and estimated $(\Delta V/V)$ [14]. The size effect $(\Delta V/V)Z_H$ is significant except for Zn and In. The calculated values of ΔZ show that all the simple metal (SM) impurities are negatively charged while TM impurities are positively charged.

3. Capture radii of impurities

The impurity vacancy capture radii r_t/r_v for various impurities are tabulated in the last column of table 1. The caputre radii of Ag and Mg impurities are adopted from the measurements of Rizk *et al* [15]. The starred value of capture radius for Mg impurity and capture radii for Ga and Si impurities are taken from Dworschak *et al*

Table 1. The physical parameters for Al alloys. Z_I are realistic valencies of impurities, Z_H is host ion valency, $(\Delta V/V)$ is lattice dilation, ΔZ are the effective charges on impurities and (r_t/r_v) are the relative capture radii of impurities.

Impurity	Z_I	$(\Delta V/V)Z_H$	ΔZ	(r_t/r_v)
Ag	1	0·14	−2·14	$0{\cdot}60 \pm 0{\cdot}05$[a]
Cu	1	−0·56	−1·44	
Mg	2	0·60	−1·60	$0{\cdot}33 \pm 0{\cdot}05$[a]
				$0{\cdot}43 \pm 0{\cdot}05$*[b]
				(0·2)
Zn	2	−0·08	−1·92	$(0{\cdot}57 \pm 0{\cdot}05)$[d]
				$(0{\cdot}75 \pm 0{\cdot}05)$
Ga	1	0·27	−2·27	$0{\cdot}65 \pm 0{\cdot}05$[b]
In	2	0·0	−1·0	
Si	2	−0·26	−0·74	0·50[b]
Ge	2	0·27	−1·27	$(0{\cdot}43 \pm 0{\cdot}05)$[d]
Sn	2	0·86	−1·86	
Cd	2	−0·55	−0·45	
Ti	3	−0·82	0·82	$0{\cdot}40 \pm 0{\cdot}10$[c]
V	2	−0·83	0·17	$0{\cdot}15 \pm 0{\cdot}05$[c]
Cr	2	−1·59	0·59	$0{\cdot}35 \pm 0{\cdot}05$[c]

[a]Rizk *et al* [15]; [b]Dworschak *et al* [16]; [c]Maury *et al* [17]; [d]Normalized values of [16]

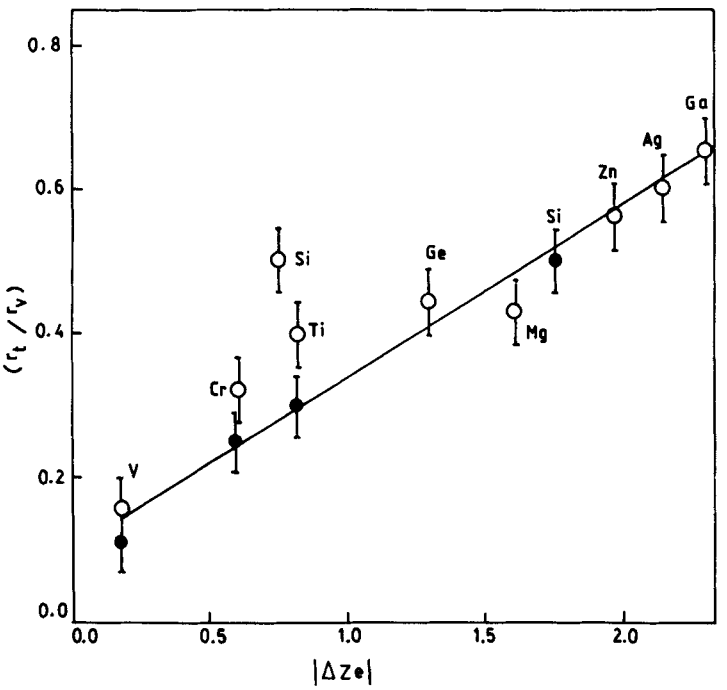

Figure 1. (r_t/r_v) vs $|\Delta Ze|$ for dilute alloys of Al.

[16]. Maury *et al* [17] pointed out that the results of Dworschak *et al* [16] for TM impurities need a further analysis. Maury [18] found that the capture radii for Cr, V and Ti impurities are $0{\cdot}35 \pm 0{\cdot}05$, $0{\cdot}15 \pm 0{\cdot}05$ and $0{\cdot}40 \pm 0{\cdot}10$ respectively. These values are adopted in table 1. Dworschak *et al* [16] evaluated the capture radii for Ag, Ge, Mg and Zn impurities as 2·2, 1·6, 0·74 and (2·8, 2·1) respectively at 540 K. These values are consistently higher for reasons discussed by Prakash and Lucasson [11], than those obtained by Rizk *et al* [15]. Therefore we normalized these values with respect to capture radius of Ag impurity obtained by Rizk *et al* [14]. These normalized capture radii are tabulated in table 1 in brackets.

The results for capture radii for different impurities versus the magnitude of effective charges $|\Delta Ze|$ on impurities are plotted in figure 1. The corresponding error bars are also shown there. An acceptable correlation is found between the capture radii and $|\Delta Ze|$ for all SM impurities except Si. However if Si is taken as monovalent, the correlation is almost perfect. This justifies the renormalization of capture radii of Zn and Ge impurities. The capture radii of TM impurities also show a linear correlation with $|\Delta Ze|$ although the slope is different from that for SM impurities. If the capture radii of TM impurities are reduced uniformly say by 25%, a reasonable linear correlation is established. This suggests that the capture radii of impurities are proportional to the magnitude of total perturbation caused by both the valence and size effects and not only the valence or size effect as discussed earlier [16].

4. Spherical solid model and non-linear screening

The Kohn-Sham density-functional formalism is used to calculate the screening of impurity atom by the conduction electrons. A set of wave functions ψ_i with energy

eigenvalues ε_i is generated by solving the Schrödinger equation

$$[-\tfrac{1}{2}\nabla^2 + V(\mathbf{r})]\psi_i(\mathbf{r}) = \varepsilon_i\psi_i(\mathbf{r}), \tag{5}$$

where

$$V(\mathbf{r}) = \phi(\mathbf{r}) + V_{ss}(\mathbf{r}) + \mu_{xc}(n, r). \tag{6}$$

$\phi(\mathbf{r})$ is the electrostatic potential due to induced charge density defined as

$$\phi(\mathbf{r}) = \int \frac{d\mathbf{r}'[n(\mathbf{r}') - n_+(\mathbf{r}')]}{|\mathbf{r} - \mathbf{r}'|}, \tag{7}$$

where

$$n(\mathbf{r}) = \Sigma|\psi_i(\mathbf{r})|^2, \tag{8}$$

and for the substitutional impurity

$$n_+(\mathbf{r}) = n_0\theta(\mathbf{r} - \mathbf{R}_{ws}) + Z'\delta(\mathbf{r}). \tag{9}$$

Here $n_0 (= 3/(4\pi r_s^3))$ is the uniform electronic charge density, r_s is interelectronic distance, R_{ws} is Wigner-Seitz cell radius and $\theta(r)$ is the unit step function.

The spherical solid potential $V_{ss}(r)$ is given as

$$V_{ss}(\mathbf{r}) = -\frac{1}{4}\int d\Omega \sum_n{}' w(\mathbf{r} - \mathbf{R}_n^0) + \int \frac{d\mathbf{r}' n_0\theta(\mathbf{r} - \mathbf{R}_{ws})}{|\mathbf{r} - \mathbf{r}'|}. \tag{10}$$

In (10) the first term in the spherical average of bare ion pseudopotential at $\mathbf{r}$ and the second term is the potential due to uniform positive charge background. The last term on rhs of (6) is the exchange-correlation potential. In the local density approximation it is given as

$$\mu_{xc}(n, \mathbf{r}) \simeq \frac{d}{dn}[n\varepsilon_{xc}(n) - \mu_{xc}(n)] - \mu_{xc}(n_0), \tag{11}$$

where ε_{xc} is the exchange-correlation energy per electron of electron gas of density $n(r)$ and $\mu_{xc}(n_0)$ is the exchange-correlation potential for density n_0. We used the following parametrized form of ε_{xc} in our calculations [18]

$$\varepsilon_{xc}(R_s) = -\frac{0{\cdot}9163}{R_s} - 0{\cdot}112 + 0{\cdot}0335\ln R_s - \frac{0{\cdot}02}{0{\cdot}1 + R_s}, \tag{12}$$

where $R_s = (3/(4\pi n(r))^{1/3}$ and $\mu_{xc}(n_0)$ is subtracted to get convergence of $\mu_{xc}(n, r)$ at large r.

We used the Ashcroft model potential for the host ions and calculated $V_{ss}(r)$ for substitutional impurity in the same manner as discussed in [9]. The final expression is given as

$$V_{ss}(r) = V_{ss}(0) - \frac{2\pi n_0}{3}\left(r^2 + \frac{2R_{ws}^3}{r}\right)\theta(r - R_{ws}) -$$

$$-\begin{cases} \sum_n{}' \dfrac{Z_H}{R_n^0}\left(\dfrac{r + R_n^0 - r_c}{2r} - 1\right); & |\mathbf{R}_n^0 - \mathbf{r}_c| \leqslant r \leqslant |\mathbf{R}_n^0 + \mathbf{r}_c| \\ \sum_n{}' \left(\dfrac{Z_H}{|\mathbf{r}|} - \dfrac{Z_H}{|\mathbf{R}_n^0|}\right); & r > |\mathbf{R}_n^0 + \mathbf{r}_c| \end{cases} \tag{13}$$

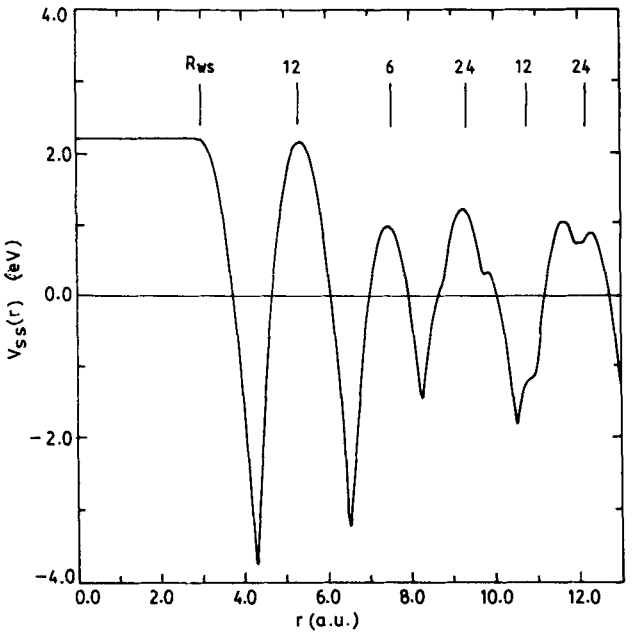

Figure 2. Spherical solid potential $V_{ss}(r)$ versus r for Al around substitutional site. The positions and number of NNs are indicated. R_{ws} is Wigner-Seitz radius.

where

$$V_{ss}(0) = \frac{Z_H \alpha_{EW}}{R_{WS}} - 2\pi n_0 R_{ws}^2 \theta(R_{ws} - r). \tag{14}$$

and r_c is potential parameter. Here $\alpha_{EW} = 1{\cdot}79172$ is used for fcc structure. For convergence purpose a constant potential $V_{ss}(r \to \infty) = 3r_c^2/2r_s^3$ is subtracted from (13). The results for Al are shown in figure (2). $V_{ss}(r)$ is found constant for $r < R_{ws}$ as given in (14). $V_{ss}(r)$ has the maxima at the lattice sites and minima between two sites and consists of both attractive as well as repulsive characteristics.

Equation (5) for spherically symmetric potential can be written as

$$\left(-\frac{1}{2}\frac{\partial^2}{\partial r^2} + V(r) + \frac{l(l+1)}{2r^2} \right) rR_{lk}(r) = \varepsilon_k rR_{lk}(r) \tag{15}$$

where $rR_{lk}(r)$ is the radial wavefunction, $\varepsilon_k = k^2/2$, $\mathbf{k}$ is the electron wavevector and l is the angular momentum (atomic units are used). At large distances

$$rR_{lk}(r) \simeq j_l(kr)\cos\delta_l - n_l(kr)\sin\delta_l \tag{16}$$

where j_l and n_l are the spherical Bessel and Neumann functions of order l respectively and δ_l are the scattering phase shifts. For a bound state the energy $\varepsilon_b < 0$ and the asymptotic form of radial wavefunction is

$$rR_b(r) \sim e^{-k_0 r} \tag{17}$$

where

$$k_0 = (-2\varepsilon_b)^{1/2}.$$

we calculate the change in charge density for convergence purpose as

$$\delta n(r) = n(r) - n_0 = \frac{1}{\pi^2} \int_0^{k_F} dk\, k^2 \sum_{l=0}^{\infty} (2l+1)[R_{lk}^2(r) - j_l^2(kr)] + 2|R_b|^2. \quad (18)$$

The sum over l in (18) converges as the effective potential is localized. Equations (15–18) are solved self-consistently following the procedure suggested by Manninen *et al* [20]. The electrostatic potential $\phi(r)$ obtained by solving the Poisson equation is given as

$$\phi^i(r) = -\frac{1}{4\pi} \int \frac{d\mathbf{r}' e^{-k_{TF}|\mathbf{r}-\mathbf{r}'|}}{|\mathbf{r}-\mathbf{r}'|} (4\pi[Z\delta(\mathbf{r}') - n^{i-1}(\mathbf{r}') + n_0] - k_{TF}^2 \phi^{i-1}(\mathbf{r}'))$$

$$+ \begin{cases} \dfrac{4\pi n_0}{k_{TF}^3 r}[k_{TF} r - \sinh(k_{TF} r)(1 + k_{TF} R_{ws}) e^{-k_{TF} R_{ws}}]; & r < R_{ws} \\ \dfrac{4\pi n_0 e^{-k_{TF} r}}{k_{TF}^3 r}[k_{TF} R_{ws} \cosh(k_{TF} R_{ws}) - \sinh(k_{TF} R_{ws})]; & r > R_{ws}. \end{cases} \quad (19)$$

Here i and $(i-1)$ correspond to the number of iterations in the self-consistent solution and $(1/k_{TF})$ is Thomas-Fermi screening length. Equation (19) is mathematically correct when $\phi^i(\mathbf{r}) = \phi^{(i-1)}(\mathbf{r})$. In this procedure the Coulombic tail, if persists, gets truncated due to exponential term. The self-consistency is achieved within about 0·1 % in charge density. The radial integration of (18) is carried out by Fox and Goodwin method in the steps of 0·1 a.u. up to 19·5 a.u. The phase shifts sum is performed up to $l = 14$. It is found that the charge density and hence the potential remains converged within the limits of accuracy if $V_{ss}(r)$ is included up to $r = 8$ a.u.

The calculations are carried out in two steps. In the first step the calculations are performed for the perfect crystal by putting $n(r) = n_H(r)$, $Z' = Z_H$, $\delta n(r) = \delta n_H(r) = n_H(r) - n_0$, in eqs (5–10) and (15–19). The self-consistently calculated $V_H(r)$ and $\delta n_H(r)$ are retained. In the second step the calculations are performed for the defect crystal with an impurity at the origin. $n(r) = n_I(r)$, $Z' = Z'$ and $\delta n_I(r) = n_I(r) - n_0$ are used in eqs (5–10) and (15–19). The self-consistently calculated $V_I(r)$ and $\delta n_I(r)$ are obtained. However the Friedel sum rule

$$\Delta Z = \frac{2}{\pi} \sum_l (2l+1)\delta_l(k_F) \quad (20)$$

has to be satisfied for the defect crystal with the help of calculated phase shifts. The differences

$$\delta V_i(r) = V_I(r) - V_H(r) \quad (21)$$

and

$$\delta n_i(r) = n_I(r) - n_H(r) \quad (22)$$

give the host-impurity potential and the impurity induced charge density respectively.

5. Host-impurity potential

The self-consistently calculated host-impurity potentials given by (21) are shown in figure 3 for *Al*Cd, *Al*Si, *Al*In and *Al*Ge alloys. The inset shows the potentials on the

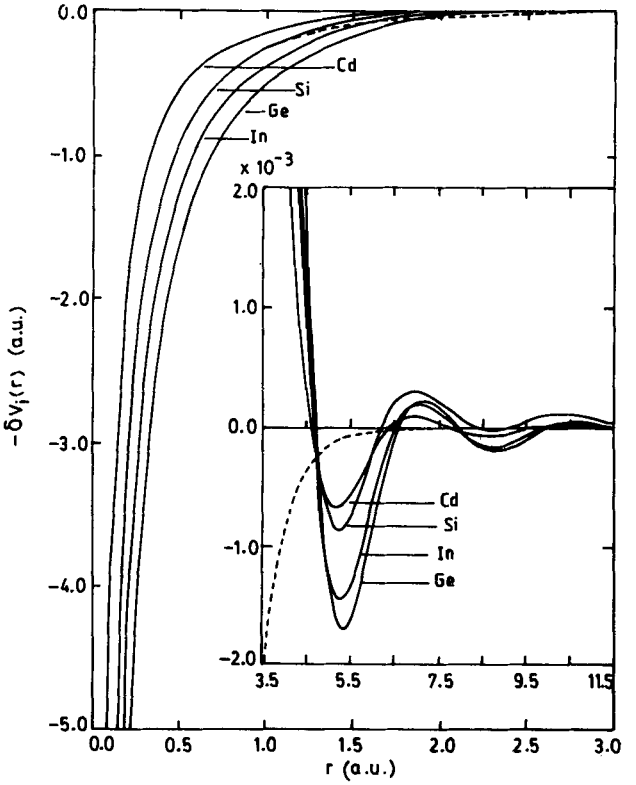

Figure 3. The host-impurity potential $\delta V_i(r)$ versus r for Al(Cd, Si, In, Ge) alloys. The inset shows Friedel oscillations. The dashed line represents the potential obtained from Eq. (23) for *Al*Si.

enhanced scale at larger distances from the impurity. The magnitude of potentials for *Al*(Cd, Si, In, Ge) are in the decreasing order.

The $\delta V_i(r)$ are repulsive for $r < 2{\cdot}5$ a.u. for *Al*Cd, *Al*Si, *Al*In and *Al*Ge alloys and oscillatory afterwards. The relative comparison shows that $\delta V_i(r)$ are proportional to effective charges of impurities at smaller r while at larger r these have Friedel oscillations. It is found that $V_{ss}(r)$ reduces the amplitude of oscillations and shifts the position of first minimum of $\delta V_i(r)$ at the 1NN site of impurity. The ranges of attractive and repulsive potentials are also altered.

We express these potentials in the analytical form [21]

$$\delta V_i(r) = -\Delta Z\left(1+\frac{\beta r}{2}\right)\exp(-\beta r)/r. \tag{23}$$

The parameter β is determined by the method of least square fit for each alloy. These values of β are given in table 2. The potential obtained from (23) is shown by dashed line for *Al*Si in figure 3. For $r < 1{\cdot}5$ a.u. eq. (23) coincides with the calculated $\delta V_i(r)$. At larger distances the potential obtained by (23) decays exponentially and there are no oscillations. Equation (23) is quite useful in determining the physical properties where the interactions from the first few neighbors of impurity are dominant.

Table 2. The calculated and experimental results for Al alloys. $\Delta\rho$ is residual resistivity, Δn_s is the excess charge in the impurity Wigner-Seitz cell, E_{se} is self-energy and β is the potential parameter. The lattice parameter $a = 7{\cdot}64$ a.u. and Ashcroft potential parameter $r_c = 1{\cdot}12$ a.u. are used.

Impurities	$\Delta\rho$ ($\mu\Omega$cm/at%) Cal.	Exp.	Δn_s	β	E_{se}(eV)
Cu	1·25	0·89	0·70	0·52	−0·14
Ag	0·32	1·08	1·85	1·00	−0·79
Cd	1·08	0·51	0·64	1·82	−0·03
Mg	1·22	0·36	1·44	0·64	−0·15
Zn	0·73	0·24	1·47	0·88	−0·30
Ga	0·24	0·22	1·15	1·05	−0·51
In	0·92	—	1·40	1·60	−0·15
Ge	0·92	0·79	1·43	1·51	−0·23
Si	0·98	0·60	0·85	1·70	−0·09
Sn	0·85	—	1·42	0·84	−0·27

6. Electron charge density and charge transfer

The impurity-induced electron charge densities $\delta n_i(r)/n_0$, given in (22), are shown in figure 4 for *Al*Cd, *Al*Si, *Al*In, *Cu*Ge, and *Al*Ga alloys. The Friedel oscillations are exhibited in the inset for *Al*Cd, *Al*In and *Al*Ga. The results for *Al*Ge and *Al*Si are close to *Al*In and *Al*Cd respectively. $[\delta n_i(r)/n_0]$ decreases rapidly with increase of r and shows oscillatory behavior for $r > 3{\cdot}0$ a.u. for Al(Cd, In, Ge, Si) and for $r > 4{\cdot}0$ a.u. for *Al*Ga. Thus Ga impurity is screened up to larger r. The $V_{ss}(r)$ has reduced the amplitude of Friedel oscillations and displaced the positions of the minima and maxima due to shell periodic character.

The solution of Poisson equation for $\delta V_i(r)$ given in (23) gives

$$\delta n_i(r) = (\Delta Z \beta^3/8\pi)\exp(-\beta r). \tag{24}$$

Equation (24) underestimates $\delta n_i(r)$ at the impurity site. The impurity self-energy $E_{se} = [-3(\Delta Z)^2\beta/32]$ is also calculated [10] for all the impurities and these results are tabulated in table 2. The self-energy is minimum for *Al*Cd and hence the stable solid solution and the minimum for *Al*Ag and hence the least stable solid solution.

We also calculated the net electronic charge in the impurity Wigner-Seitz cell by integrating $\delta n_i(r)$ from 0 to R_{ws}. These values are also tabulated in table 2 as Δn_s. The charge transfer is estimated by comparing Δn_s with Z_I. It is found the Cu, Cd, Mg, Zn, In, Ge, Si and Sn impurities transfer the charge to Al host while Ag and Ga impurities gain the charge from host. The calculations of Deutz *et al* [22] suggest that these impurities gain the charge of order of 2–4%. This difference is due to consideration of bound states and inclusion of size effect. The size effect is not included in the calculations of Deutz *et al* [22].

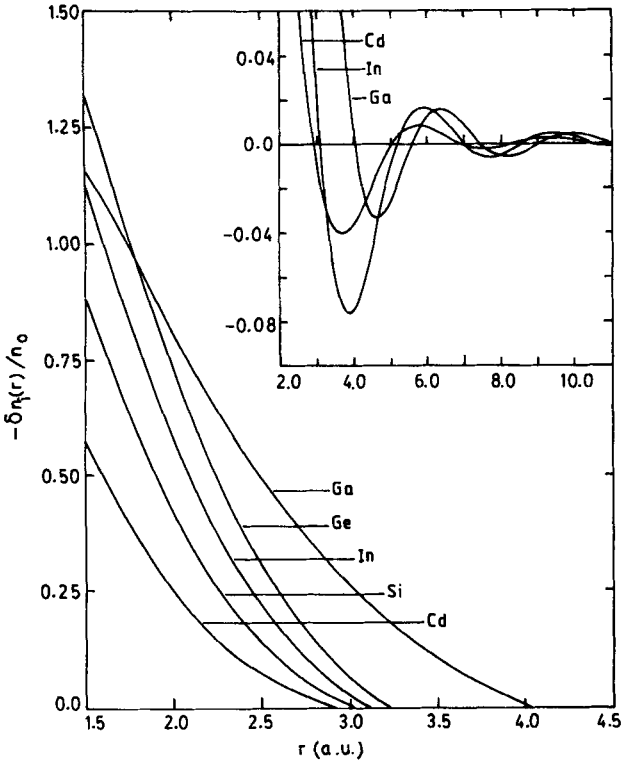

Figure 4. The impurity-induced normalized charge density $(\delta n_i(r)/n_0)$ versus r for *Al*(Cd, Si, In, Ge, Ga) alloys. The inset shows Friedel oscillations.

7. Scattering phase shifts and residual resistivity

The scattering phase shifts obtained in the self-consistent calculations of $V_l(r)$ and $n_l(r)$ by satisfying the Friedel sum rule are tabulated in table 3 up to $l = 9$. The higher order phase shifts are found negligibly small. The magnitude of the phase shifts is oscillatory. This is due to the inclusion of $V_{ss}(r)$ [2]. The p, d and f scattering phase shifts are mainly due to lattice effects through $V_{ss}(r)$. Using these phase shifts the residual resistivity is estimated with the help of following expression [10].

$$\Delta\rho = \frac{2{\cdot}732}{k_F Z_H}\left[\sum_{l=0}^{14}(l+1)\sin^2(\delta_l - \delta_{l+1})\right] \tag{25}$$

The calculated values of $\Delta\rho$ are given in table 2. The agreement with the experimental results is just qualitative. A relative comparison with the results of Mahajan and Prakash [2] shows that the introduction of $V_{ss}(r)$ enhances $\Delta\rho$. In fact $\Delta\rho$ involves a careful calculation of electron-phonon matrix element and anisotropy of Fermi surface [23]. These effects are not included in (25).

8. Electric field gradient

The total change in crystal potential due to insertion of a substitutional impurity is [24]

Table 3. The phase shifts evaluated at the Fermi surface ($E = E_F$) for Al alloys.

Phase shifts	Impurities									
	Cu	Ag	Cd	Mg	Zn	Ga	In	Ge	Si	Sn
δ_0	1·0548	−0·2287	2·3302	0·8291	0·2343	−0·4873	2·0062	1·8466	2·1610	0·3567
δ_1	−0·5343	−0·5063	0·2883	−0·5384	−0·5235	−0·4973	0·0756	−0·0212	0·1796	−0·5280
δ_2	−0·2268	−0·2168	−0·0965	−0·2292	−0·2237	−0·2113	−0·0798	−0·0776	−0·0827	−0·2256
δ_3	−0·0762	−0·0740	−0·0485	−0·7666	−0·0751	−0·0723	−0·0443	−0·0425	−0·0440	−0·0756
δ_4	0·0054	0·0055	0·0117	0·0055	0·0061	0·0062	0·0116	0·0115	0·0132	0·0059
δ_5	0·0040	0·0034	0·0046	0·0042	0·0042	0·0039	0·0042	0·0040	0·0057	0·0042
δ_6	−0·0049	−0·0054	−0·0052	−0·0048	−0·0048	−0·0050	−0·0055	−0·0057	−0·0044	−0·0048
δ_7	−0·0025	−0·0028	−0·0026	−0·0025	−0·0024	−0·0025	−0·0028	−0·0030	−0·0022	−0·0025
δ_8	−0·0003	−0·0003	−0·0002	−0·0002	−0·0002	−0·0002	−0·0003	−0·0004	−0·0001	−0·0002
δ_9	0·0001	0·0001	0·0002	0·0001	0·0001	0·0002	0·0001	0·0001	0·0002	0·0001

$$\Delta\Phi_{\mathrm{H}}(\mathbf{r}) = \Delta\phi_{\mathrm{I}}(\mathbf{r}) + \Delta\phi_{\mathrm{H}}(\mathbf{r}) \tag{27}$$

where

$$\Delta\phi_{\mathrm{I}}(r) = \phi_{\mathrm{I}}(r) - \phi_{\mathrm{H}}(r) \tag{28}$$

and

$$\Delta\phi_{\mathrm{H}}(\mathbf{r}) = \sum_{n}{}' [\phi_{\mathrm{H}}(\mathbf{r} - \mathbf{R}_n) - \phi_{\mathrm{H}}(\mathbf{r} - \mathbf{R}_n^0)]. \tag{29}$$

Here $\phi_{\mathrm{H}}(r)$ and $\phi_{\mathrm{I}}(r)$ are self-consistent interatomic potentials for host and impurity atoms respectively. $\mathbf{R}_n^0$ and $\mathbf{R}_n$ are the undisplaced and displaced positions of the host atom respectively. $\Delta\phi_{\mathrm{I}}(\mathbf{r})$ involves only one host and one impurity atom and arises from the valence difference. $\Delta\phi_{\mathrm{H}}(\mathbf{r})$ arises from the strain field and involves the entire lattice.

The EFG tensor $\mathbf{V}$ at $\mathbf{r} = \mathbf{R}_m$, the mNN of impurity, is obtained by computing the second derivative of $\Delta\Phi_{\mathrm{H}}(\mathbf{r})$ which is given as

$$\underset{\sim}{\mathbf{V}}(\mathbf{R}_m) = \underset{\sim}{\mathbf{V}}^{\mathrm{v}}(\mathbf{R}_m) + \underset{\sim}{\mathbf{V}}^{\mathrm{s}}(\mathbf{R}_m) \tag{30}$$

where the valence EFG

$$\mathbf{V}^{\mathrm{v}}(\mathbf{R}_m) = (1 - \gamma_\infty)[\nabla\cdot\nabla\{\Delta\phi_{\mathrm{I}}(\mathbf{r})\}]_{\mathbf{r}=\mathbf{R}_m} \tag{31}$$

and the size EFG

$$\mathbf{V}^{\mathrm{s}}(\mathbf{R}_m) = (1 - \gamma_\infty)[\nabla\cdot\nabla\{\Delta\phi_{\mathrm{H}}(\mathbf{r})\}]_{\mathbf{r}=\mathbf{R}_m}. \tag{32}$$

$(1 - \gamma_\infty)$ is Sternheimier antishielding factor [25].

The displaced positions of host atoms are calculated in the continuum model of the lattice and these are given as [9]

$$\mathbf{R}_m = \sqrt{m}R_1^0 + \frac{(1+\sigma)}{4\pi(1-\sigma)}\frac{\Omega_0}{(\sqrt{m}R_1^0)^2}\left(\frac{1}{a}\frac{\mathrm{d}a}{\mathrm{d}c}\right) \tag{33}$$

where Ω_0 is the atomic volume of the host lattice. σ is Poisson ratio and $(1/a)\,(\mathrm{d}a/\mathrm{d}c)$ is the fractional change in lattice parameter 'a' per unit concentration. The total EFG is obtained by adding the corresponding Cartesian components of the valence and size EFGs i.e.

$$V_{\alpha\beta}(\mathbf{R}_m) = V^{\mathrm{v}}_{\alpha\beta}(\mathbf{R}_m) + V^{\mathrm{s}}_{\alpha\beta}(\mathbf{R}_m). \tag{34}$$

The components of traceless EFG tensor $\mathbf{q}$ are given as

$$q_{\alpha\beta} = V_{\alpha\beta} - (1/3)\sum_{\alpha} V_{\alpha\alpha}. \tag{35}$$

The (3×3) matrix of $q_{\alpha\beta}$ is diagonalized to obtain the eigenvalues and eigenvectors. The eigenvalue corresponding to eigenvector parallel to the line joining the impurity and host atom is taken as

$$q_{ZZ} = q_{\parallel}. \tag{36}$$

Other two components are written as

$$q_{YY} = q_{\perp} \text{ and } q_{XX} = q_{xx}. \tag{37}$$

In general $|q_{ZZ}| \geqslant |q_{YY}| \geqslant |q_{XX}|$ and the asymmetry parameter η is defined as

$$\eta = |q_{XX} - q_{YY}|/|q_{ZZ}|. \tag{38}$$

In the fcc lattice $\mathbf{V}^{\mathrm{v}}$ and $\mathbf{V}^{\mathrm{s}}$ are similar matrices at the 1NN and 2NN sites. Therefore these can be diagonalized separately and eigenvalues of the same eigenvectors can be added.

To calculate the valence EFGs $\Delta\phi_1(\mathbf{r}) = (1/e)\delta V_i(\mathbf{r})$ is calculated from (21) and it is used in (31). The differentiation is carried out numerically at the displaced positions of 1NNs and 2NNs of impurities. These values are used in (35) to get the traceless EFG components $q^{\mathrm{v}}_{\alpha\beta}$. $\gamma_\infty = -2{\cdot}59$ is used [8].

To evaluate the size EFGs, we have adopted the continuum model of the lattice. In this model size EFG is given as [26]

$$q^{\mathrm{s}}_{\alpha\beta} = (1/e)\left[(F_{11} - F_{12})\delta_{\alpha\beta}\left\{\varepsilon_{\alpha\alpha} - \frac{1}{3}\sum_{\gamma}\varepsilon_{\gamma\gamma}\right\} + 2F_{44}(1 - \delta_{\alpha\beta})\varepsilon_{\alpha\beta}\right] \tag{39}$$

where $\varepsilon_{\alpha\beta}$ are the components of a symmetric strain tensor and $F_{\alpha'\beta'}$ are the components of a fourth order tensor, $\alpha', \beta' = 1, 2 \ldots 6$. For a cubic crystal $F_{11} = -2F_{22} = -2F_{44}$. F_{11} is taken from the calculations of Pal *et al* [27]. The following components are at the 1NN site

$$q^{\mathrm{s}}_{XX} = -2q^{\mathrm{s}}_{YY} = -2q^{\mathrm{s}}_{ZZ} = \frac{1}{3e}(3D_2/R_1^3)(F_{11} - F_{12})$$

$$q^{\mathrm{s}}_{YZ} = -\frac{1}{2e}(3D_2/R_1^3)F_{44};$$

and

$$q^{\mathrm{s}}_{XY} = q^{\mathrm{s}}_{ZX} = 0. \tag{40}$$

Here

$$D_2 = \frac{a^3}{16\pi}\left(\frac{1}{a}\frac{\mathrm{d}a}{\mathrm{d}c}\right)\left(\frac{1+\sigma}{1-\sigma}\right). \tag{41}$$

Similarly at the 2NN site

$$q^{\mathrm{s}}_{XX} = q^{\mathrm{s}}_{YY} = -\frac{1}{2}q^{\mathrm{s}}_{ZZ} = \frac{1}{3e}(3D_2/R_2^3)(F_{11} - F_{22})$$

and

$$q^{\mathrm{s}}_{XY} = q^{\mathrm{s}}_{YZ} = q^{\mathrm{s}}_{ZX} = 0. \tag{42}$$

The calculated values of q^{v}_{XX}, $q^{\mathrm{v}}_{\perp}$, $q^{\mathrm{v}}_{\parallel}$ and q^{s}_{XX}, $q^{\mathrm{s}}_{\perp}$, $q^{\mathrm{s}}_{\parallel}$ at the 1NN and 2NN sites of impurity are tabulated in tables 4 and 5 respectively. The size strength parameter D_2 is increased by a factor of 7·50 for an over all agreement of EFG with the experimental value of *Al*Cu at 1NN site. The same enhancement is used for other alloys also. Such an enhancement is not introduced for the 2NN site EFG calculations. The respective components are added and the magnitude of the largest sum is taken as EFG for that particular alloy. The calculated values of η are also tabulated in table 4. η vanishes at the 2NN site. The results are compared with the experimental values. The following observations are made:

(i) At the 1NN site the valence EFG components have cylindrical symmetry while

Table 4. Calculated and experimental values of EFG $q(\text{Å}^{-3})$ and asymmetry parameter η at the 1NN site in Al alloys. v, s, t denote valence, size and total EFGs. Underlined values are the principal components of net EFG (q_{cal}).

Impurities	EFG Components	q_{xx}	$q_\perp$	q	$\lvert q_{cal}\rvert$ [exp]	η_{cal} [exp]
Cu	v	0·025	0·025	−0·051	0·244	0·68
	s	0·179	−0·269	0·090	[0·297]	[0·23]
	t	0·204	0·244	0·039		
Ag	v	0·024	0·024	−0·048	0·067	0·85
	s	−0·029	0·043	−0·014	[0·218]	[0·31]
	t	−0·005	0·067	−0·062		
Cd	v	0·017	0·017	−0·033	0·243	0·56
	s	0·174	−0·260	0·087	[0·182]	[0·03]
	t	0·191	−0·243	0·054		
Mg	v	0·029	0·029	−0·059	0·273	0·03
	s	−0·162	0·244	−0·081	[0·195]	[0·07]
	t	−0·133	0·273	−0·140		
Zn	v	0·015	0·015	−0·031	0·033	0·39
	s	0·018	−0·028	0·009	[0·180]	[0·27]
	t	0·033	−0·013	−0·022		
Ga	v	0·024	0·024	−0·048	0·103	0·44
	s	−0·053	0·079	−0·026	[0·228]	[0·03]
	t	−0·029	0·103	−0·074		
Si	v	0·029	0·029	−0·059	0·095	0·47
	s	0·066	−0·100	0·033	[0·282]	[0·03]
	t	0·095	0·071	−0·026		
Sn	v	0·023	0·023	−0·046	0·317	0·02
	s	−0·196	0·294	−0·098	[0·266]	[0·37]
	t	−0·173	0·317	−0·144		

the size EFG components have cubic symmetry. This is due to the fact that $\Delta\phi_i(r)$ is spherically symmetric while crystal symmetry is considered in the determination of F_{11}. At the 2NN site both the valence and size EFGs are cylindrically symmetric.

(ii) At the 1NN site $q_\perp^v$ is consistently smaller than $q_\perp^s$. The maximum components are along the perpendicular direction. The calculated values of EFGs at 1NN are in agreement with the experimental values except for *Al*Ag, *Al*Zn and *Al*Si where the calculated values are smaller than the experimental values. This is due to the fact that size effect is overestimated. The size strength parameter D_2 is not varied for each alloy to get an agreement between the calculated and experimental values of EFGs. The agreement between the calculated and experimental values of η is rather uneven. This is because η depends on the cancellation of two small quantities and also divided by a small quantity.

(iii) At the 2NN site the magnitudes of EFGs are small. The maximum components are along the parallel direction. The calculated values are in agreement with the

Table 5. Calculated and experimental values of EFG $q(\text{Å}^{-3})$ at the 2NN site in Al alloys. The description is the same as that of table 4.

Impurities	EFG Components	q_{xx}	$q_{\perp}$	q	$\lvert q_{cal}\rvert$ [exp]
Cu	v	−0·011	−0·011	0·022	0·005
	s	0·008	0·008	−0·017	[<0·020]
	t	−0·003	−0·003	0·005	
Ag	v	−0·008	−0·008	0·016	0·019
	s	−0·002	−0·002	0·003	[0·032]
	t	−0·010	−0·010	0·019	
Cd	v	0·0	0·0	0·001	0·015
	s	0·080	0·080	−0·016	[−]
	t	0·080	0·080	−0·015	
Mg	v	−0·011	−0·011	0·022	0·038
	s	−0·008	−0·008	0·016	[<0·020]
	t	−0·019	−0·019	0·038	
Zn	v	−0·010	−0·010	0·019	0·017
	s	0·001	0·001	−0·002	[<0·020]
	t	−0·009	−0·009	0·017	
Ga	v	−0·008	−0·008	0·016	0·021
	s	−0·002	−0·002	0·005	[<0·020]
	t	−0·010	−0·010	0·021	
Si	v	0·0	0·0	−0·001	0·007
	s	0·003	0·003	−0·006	[<0·020]
	t	0·003	0·003	0·007	
Sn	v	−0·010	−0·010	0·020	0·039
	s	−0·009	−0·009	0·019	[0·049]
	t	−0·019	−0·019	0·039	

experimental values except for *Al*Ag and *Al*Sn. The calculated values of EFGs for these alloys are lower than experimental values.

In the present calculations the valence EFG does not involve any core enhancement factor and there are no restrictions of asymptotic and preasymptotic limits of charge distributions. In the earlier calculations [28] the valence EFG was evaluated with the help of asymptotic charge distribution involving core enhancement factor. In the present calculations valence EFG is evaluated directly from $\Delta V_i(r)$ without introducing any parameter. The size EFG at the 1NN sites involves a unified size strength parameter and no size strength parameter is introduced at the 2NN sites. The general agreement of the calculated EFGs and η with the experimental values is as good as found in earlier calculations [28]. Thus we conclude that our simplified model does explain the local electronic structure of dilute alloys of Al.

9. Discussion

Our calculations are based on a simple but realistic physical model for dilute alloys. The effective valency is determined considering bound states and rigid ion model.

The lattice effects are included through SSM and the lattice distortion through Blatt correction. In a dilute alloy the host ion configuration may also alter, however this effect is not included here. The results may further be improved by including more realistic periodic potential. However this leads to intractable non-linear screening calculations [28]. The host-impurity potentials and impurity-induced charge densities are taken spherically symmetric in these calculations. The consideration of anisotropy of charge density may improve the results [29]. But these effects may be quite small in SM Al alloys of close packed cubic symmetry.

Acknowledgements

The authors are thankful to Dr J Singh for fruitful discussion. The financial support from Department of Atomic Energy, Bombay is also acknowledged.

References

[1] P Hohenberg and W Kohn, *Phys. Rev.* **B136**, 864 (1964)
W Kohn and L J Sham, *Phys. Rev.* **A140**, 1133 (1965)
[2] S Mahajan and S Prakash, *Phys. Status. Solidi* **B119**, 381 (1983)
[3] M Manninen and R M Nieminen, *J. Phys.* **F9**, 1333 (1979)
[4] R M Nieminen and M Pushka, *J. Phys.* **F10**, L123 (1980)
[5] S Mahajan, *Energetics of interstitial and substitutional impurities in metals* Thesis, Panjab University, Chandigarh (India) 1984
[6] S Prakash, *J. Phys.* **F8**, 2497 (1978)
[7] S D Raj, J Singh and S Prakash, *J. Phys.* **F12**, 1941 (1982)
[8] M J Ponnambalam and P Jena, *Hyperfine Int.* **20**, 65 (1984)
[9] P Singh, J Singh, S K Rattan and S Prakash, *Phys. Rev.* **B49**, 2335 (1994)
[10] P Singh and S Prakash, *Pramana – J. Phys.* **41**, 239 (1993)
[11] S Prakash and P Lucasson, *J. Phys.* **F11**, 2515 (1981)
[12] B Johnsson and N Martensson, *Phys. Rev.* **B21**, 4427 (1980)
[13] Handbook of Chemistry and Physics, The Chemical Rubber Publications, E-76 (1962)
[14] W B Pearson, *Handbook of lattice spacings and structures of metals and alloys* (Pergamon, New York, 1978)
[15] R Rizk, P Vajda, F Maury, A Lucasson, P Lucasson, C Dimitrov and O Dimitrov, *J. Appl. Phys.* **47**, 4740 (1976)
[16] F Dworschak, C Dimitrov and O Dimitrov, *J. Phys.* **F8**, L153 (1978)
[17] F Maury, A Lucasson, P Lucasson J Le Herichy, P Vajda, C Dimitrov and O Dimitrov, *Radiat Eff.* **51**, 57 (1980)
[18] F Maury, *J. Phys.* **F14**, 1395 (1984) and references therein
[19] P Vashistha and K S Singwi, *Phys. Rev.* **B6**, 8756 (1972)
[20] M Manninen, R Nieminen, P Haützarvi and J M Arpponen, *Phys. Rev.* **B12**, 4012 (1975)
[21] C A Sholl and P V Smith, *J. Phys.* **F8**, 775 (1978)
[22] J Deutz, P H Dederichs and R Zeller, *J. Phys.* **F11**, 1787 (1981)
[23] N Singh, J Singh and S Prakash, *Phys. Status Solidi* **B79**, 787 (1977) and the references therein
[24] S Prakash, J Singh and S K Rattan, *Phys. Rev.* **B48**, 6927 (1993)
[25] M H Cohen and F Reif, *Solid State Phys.* **5**, 321 (New York, Academic Press, 1957)
[26] P L Sagalyn and M N Alexander, *Phys. Rev.* **B15**, 5581 (1977)
[27] B Pal, S Mahajan, S D Raj, J Singh and S Prakash, *Phys. Rev.* **B30**, 3191 (1984)
[28] S Mahajan, B Pal and S Prakash, *Physica* **B132**, 61 (1985)
[29] J Singh, S K Rattan and S Prakash, *Phys. Rev.* **B38**, 10440 (1988)